Supporting Information: Li, Sieben *et al.*

Fig. S1

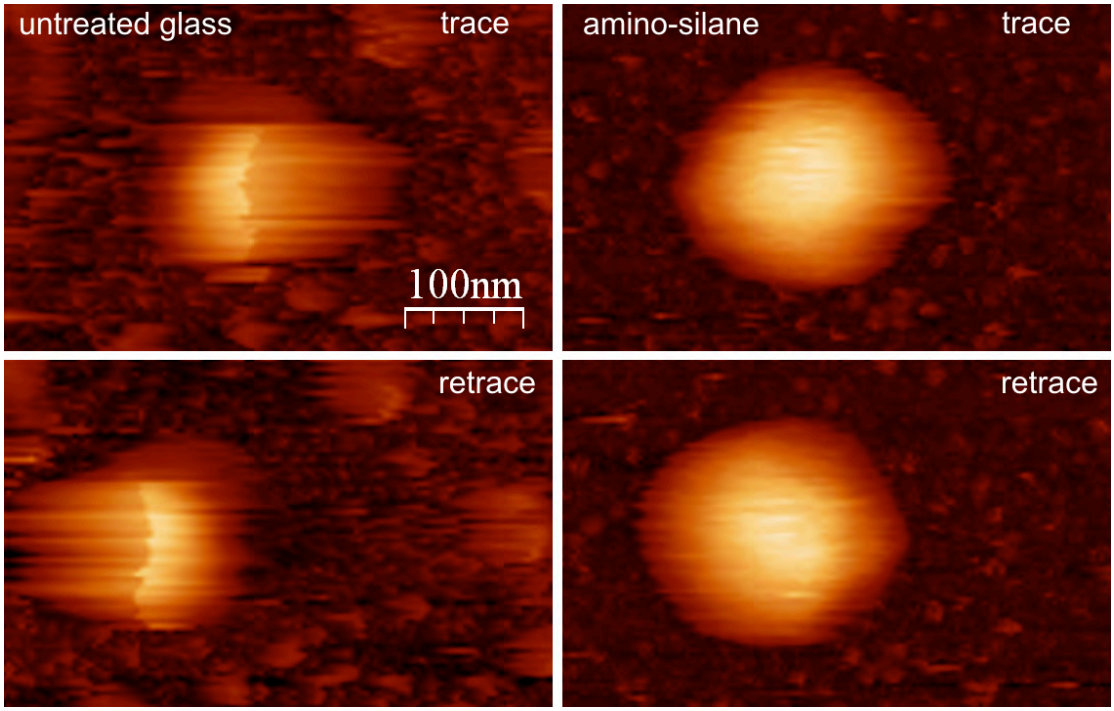

Immobilization of influenza virus particles.
We have attempted several methods to immobilize the particles to the glass coverslips. We did not succeed in attaching particles to glass surfaces that were plasma cleaned or treated with the hydrophobic hexamethyldisilazane. Only in a very few cases we could observe attachment of a virus to untreated cover slips.
Left images: The poor immobilization on untreated glass is shown by the large displacement of the particle during forward (upper image) and backward scanning (lower image).
Right images: Attachment of the virus to surfaces treated with a positively charged amino silane resulted in less motion of the particle and a shape that could be better resolved. Still, the remaining displacement between the forward and backward scans shows that the particle is not very firmly attached to the surface.
All images are shown on the same scale (z-scale = 100 nm). Both particles have a height of ~80 nm. AFM imaging was performed at low force conditions in tapping mode with a BL150 cantilever (Olympus, k=0.03 N/m, oscillated at ~ 3 nm at ~8 kHz).

Fig. S2

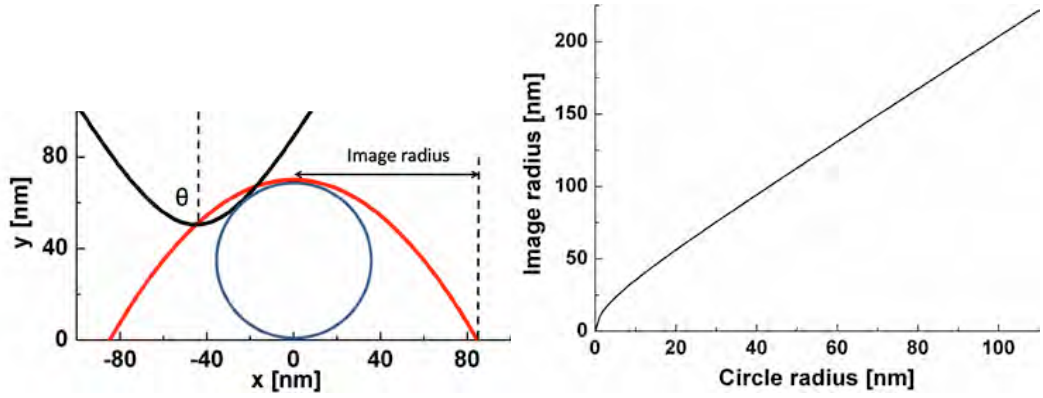

Particle selection criteria.

Because the measured stiffness can also depend on the shape of the particles, we excluded particles with an extended or flattened shape and only approximately round particles were included in the analysis.

Left graph: For each imaged virus, the height was used to calculate the expected dilation effect of imaging with a hyperbolic tip with a tip radius t_r of 20 nm and a open angle θ of 30º:

$$f(x) = \frac{1}{\tan\theta}\left(\sqrt{x^2 + \frac{t_r^{\,2}}{\tan^2\theta}} - \frac{t_r}{\tan\theta}\right)$$

Right graph: The calculated radius after dilation with the AFM tip. The width of the imaged particle is approximately twice its height, If the radius of the imaged particle deviated by less than 30 % from the expected radius, it was considered acceptable. Less then 6% of all scanned particles were excluded for further analysis based on this criterion.

Fig. S3

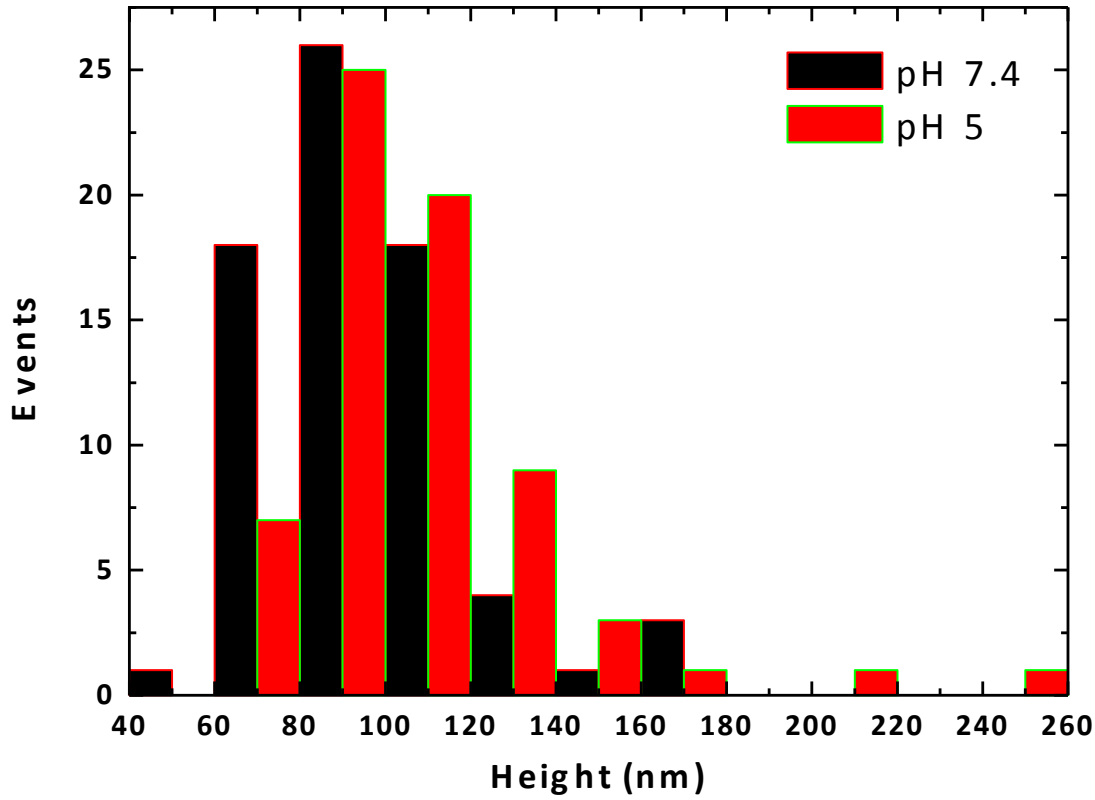

Height distribution of the tested A/X31 influenza viruses.
For each measured particle the height was measured and plotted in a histogram. At pH 7.4, 62 % of the height values are lying between 80 and 120 nm height. At pH 5.0 this is 69 %.

Fig. S4

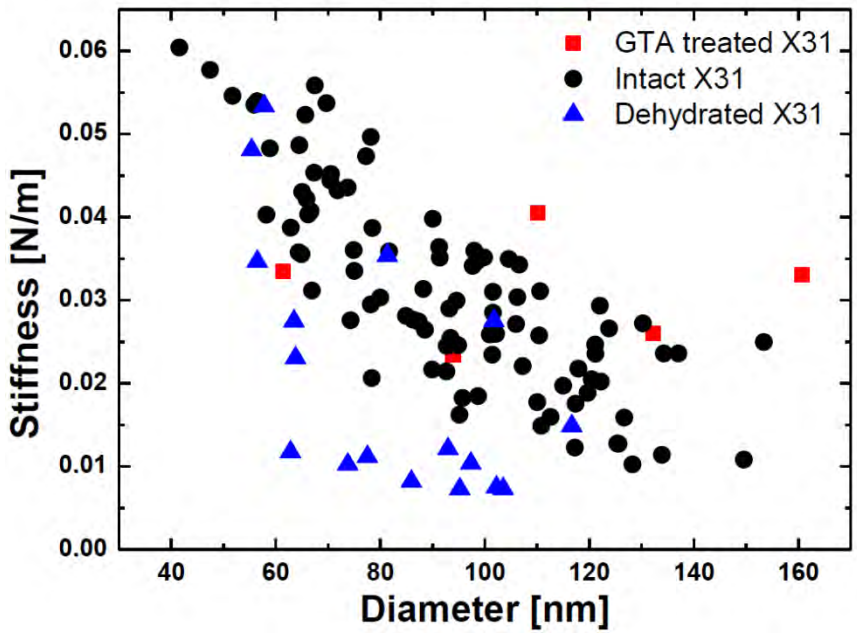

Disruption of influenza virus particles.
To test the robustness of the A/X31 influenza virus particles we subjected them to a treatment with glutaraldehyde and to a drying step followed by dehydration. The black dots show the measurements at pH 7.4 which are also presented in the main manuscript. In red, 5 particles are shown that were incubated for 20 min in presence of 2% glutaraldehyde. No drastic changes in stiffness occurred. In blue, the absorbed particles were dried for 8 hours in a vacuum desiccator and rehydrated with milli-Q water to retrieve to the concentration of the buffer. Although multiple particles seem to have (mechanically) survived this procedure, the majority shows a ~ 3-fold reduction in stiffness.

Fig. S5

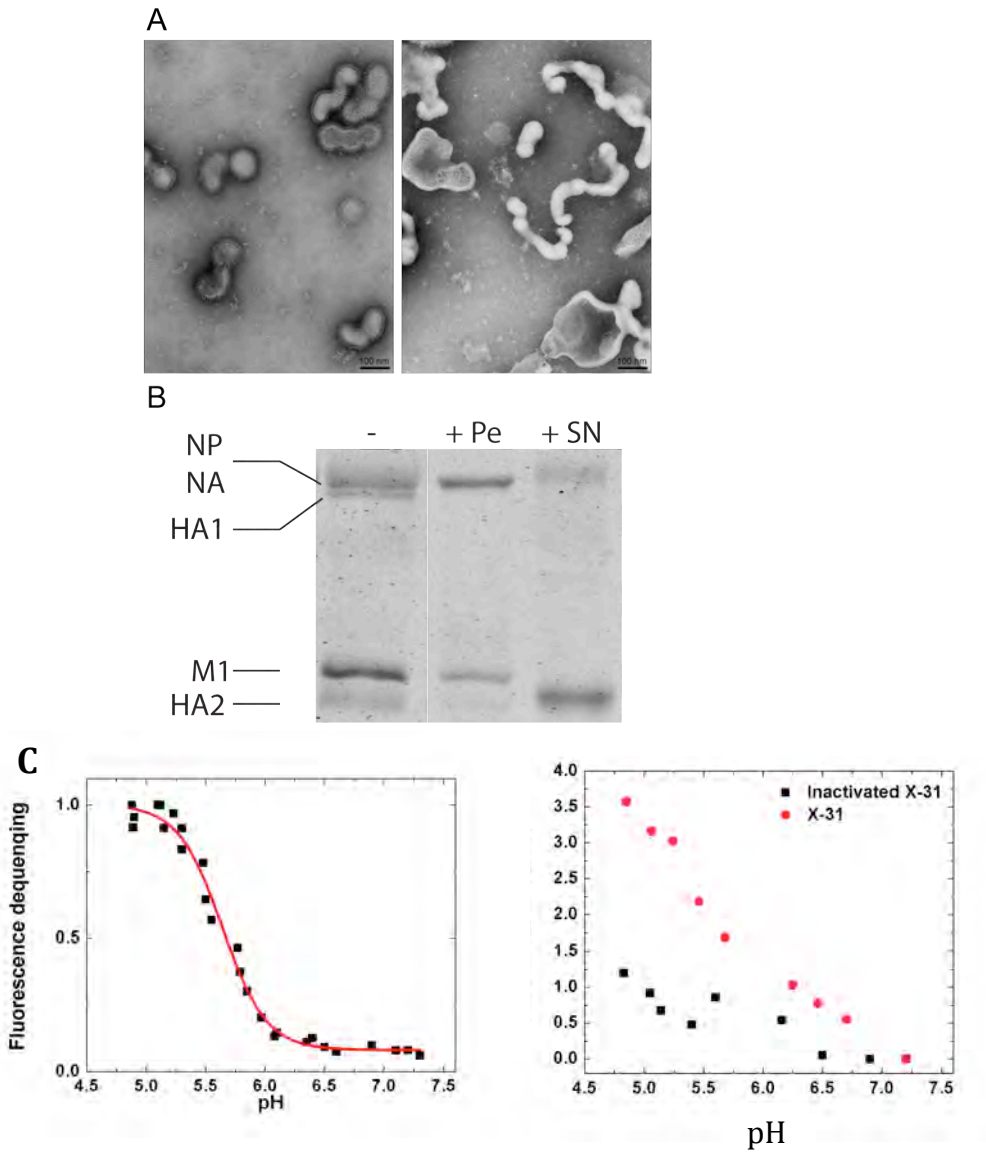

Electron microscopy and SDS-PAGE analysis of bromelain-treated influenza A viruses. (A) Electron micrographs of untreated- (left) and bromelain-treated (right) A/X31 viruses confirm the release of HA spikes after digestion. Samples of untreated or bromelain-treated influenza A virus were negatively stained with 1 % (w/v) phosphotungstic acid (PTA), pH 7.4. Bromelain-treatment yielded particles with a smooth surface, and devoid of the spikes observed at the surface of untreated virions.
(B) SDS-PAGE (reducing) analysis of bromelain-treated A/X31 viruses. The amount of un-digested HA in bromelain-treated samples was <5 %. Pellets (Pe) showed no residual HA whereas supernatants (SN) contained the expected released HA1 and HA2 polypeptides. '+' indicates the presence of bromelain.
(C) *Left:* Fusion of influenza A/X31 with ghost membranes as function of pH. Virus-cell fusion was measured by R18 dequenching 9 min after pH lowering. *Right*: The conformational change of HA within intact viruses monitored with the environment-sensitive fluorophore bis-ANS. Low-pH inactivated virus was used as control. The data were normalized to the pH 7 value. Bis-ANS binding to HA only occurred below pH 6.0.

Fig. S6

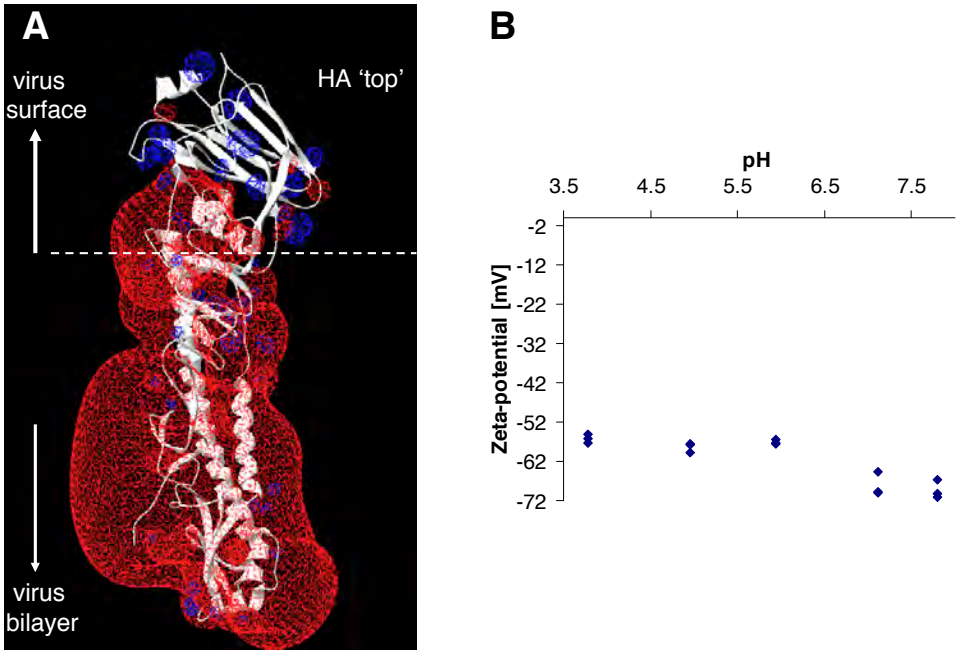

Electrostatic potential at the surface of virions and influenza virus lipid liposomes.
The interaction regime between an AFM probed surface and a scanning tip can influence force response curves, with possible pH-dependent variations (1). Since influenza virus membranes and proteins contain ionizable groups, we studied the electrostatic potential at the surface of virions and influenza virus lipid liposomes.
(A) The Coulomb electrostatic potential of the HA monomer was calculated using SPDBV using the 2VIU PDB entry. The potential of the solvent-exposed part of spike glycoproteins (HA-top) was largely positive (in blue). This was due to the presence of solvent-exposed Lysine residues, whose pKa (ca. 10) is outside of the 7.5>pH>5.0 range used in our study: Thus, the electrostatic potential at the virus surface will not vary in that range, providing that i) the conformation of HA at pH 6.0 is prefusion-like and ii) all ionization changes in HA1 at pH 6.0 are restricted to interfacial residues (2, 3).
(B) The Zeta potential of influenza liposomes was measured on a Malvern ZetaSizer Nano: A stock of liposomes at roughly 1 mM in PBS was diluted to 1/100 in an aqueous solution that was buffered to the desired pH value. Hepes 5 mM pH 7.5, Mops 5 mM pH 7.0, MES 5 mM pH 6.0, Citrate 2 mM pH 5.0, and acetate 2 mM pH 3.7 were utilized. Zetasizer measurements showed that liposomes had a significant negative potential, consistent with the presence of phosphatidylserine in the influenza virus bilayer. No drastic effect of pH on the value or sign of the potential could be observed in the investigated pH range, consistent with an observed pKa<3 or >8 for highly concentrated phosphatidylserine layers (4) (The composition of egg-purified PR8 influenza virus liposomes is described in (5); one expects phosphatidylserine to be concentrated on the cytosolic side of the plasma- and viral membrane (6)). This comforts the absence of any charge change of lipids in the pH range we investigated.

Fig. S7

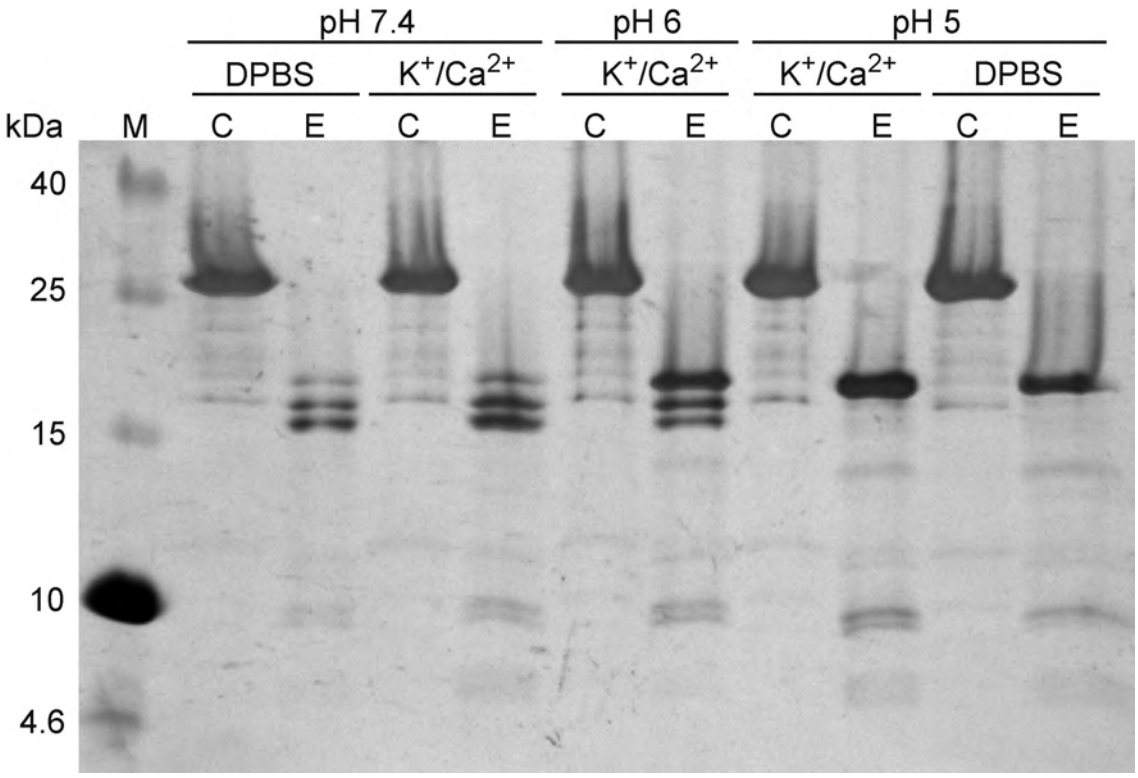

SDS-PAGE analysis of M1 after pH pre-incubation and limited proteolysis with proteinase K.
Recombinantly generated M1 was pre-incubated with either DPBS or potassium phosphate buffered saline (with high K+ and Ca2+ concentrations) at the indicated pH conditions. The different samples were subjected to proteolysis with proteinase K at a molecular enzyme-to-protein ratio of 1:100 for 20 min at RT. Enzyme-treated M1 after proteolysis (E) and the respective control samples (C), which were incubated in the absence of enzyme, are shown. M1 (28 kDa) was efficiently proteolysed at all pH and buffer conditions. The specific cleavage products of M1 were found to differ in a pH-dependent way, indicating different pH-dependent conformational states of the protein. One major cleavage product (between 15 and 25 kDa) was formed at pH 5, while two slightly smaller protein fragments arose at pH 7.4. An intermediate state, showing considerable amounts of all three cleavage products, can be observed at pH 6. The results were essentially the same when using DPBS or high K+/Ca2+ concentrations at identical pH-values. (C: control, E: enzyme-treated, M: molecular weight marker).

Fig. S8

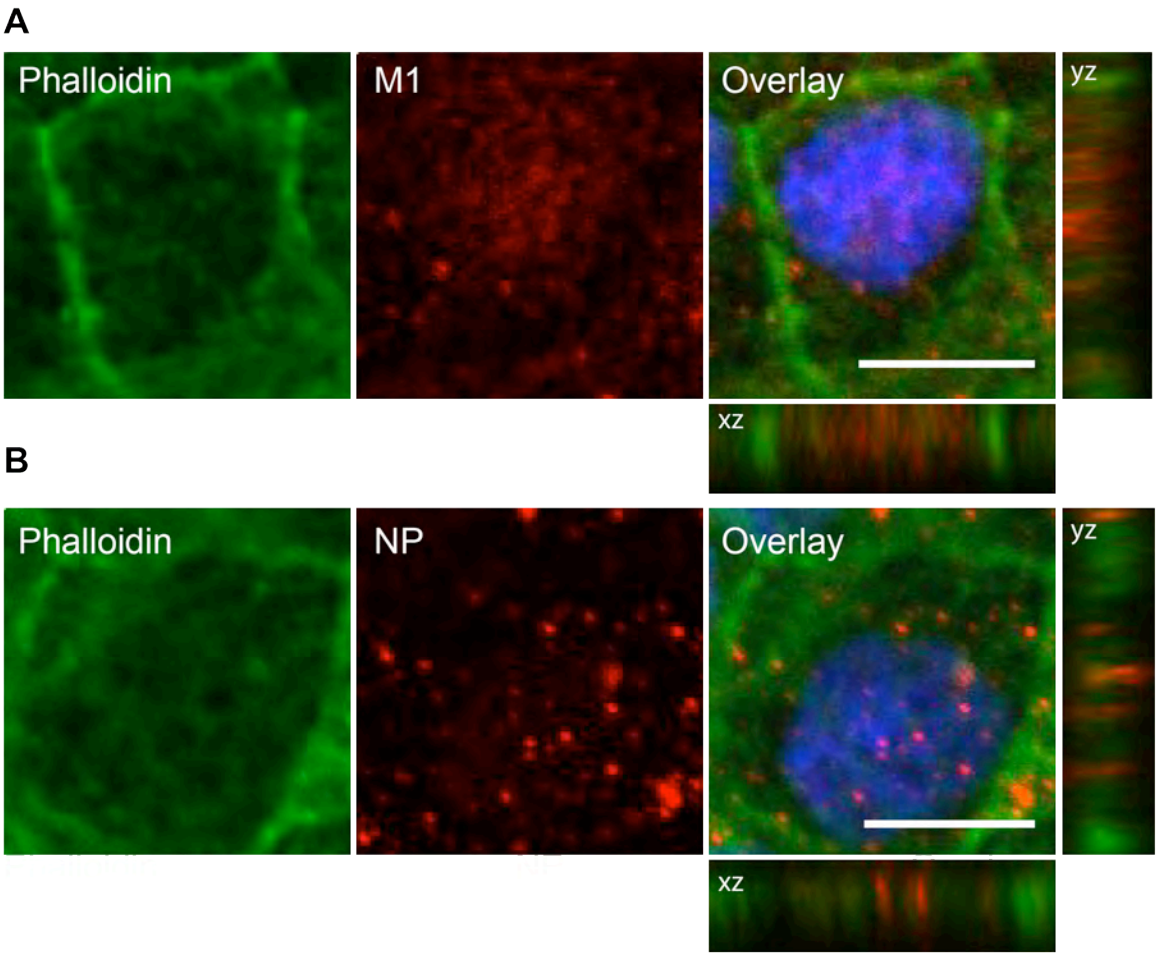

M1 and NP do not co-localize with phalloidin after acid by-pass.
Acid by-pass was conducted as described. The cells were immunostained using antibodies against the viral M1 (A) (anti-goat A647) and NP (B) (anti-mouse A647). In addition, actin was labeled using rhodamine-labeled phalloidin. Phalloidin allows identification of the cell boundaries due to cortical actin accumulation. The cells were imaged using confocal microscopy. The figure shows a central slice of the cell that allows clear identification of the cell boundaries in the phalloidin channel as well as orthogonal views from X and Y axis. NP and M1 do not co-localize with the cell boundaries and are visible inside the cell lumen. We conclude that both proteins are localized inside the cell (cytoplasm and nucleus) after acid by-pass.

Fig. S9

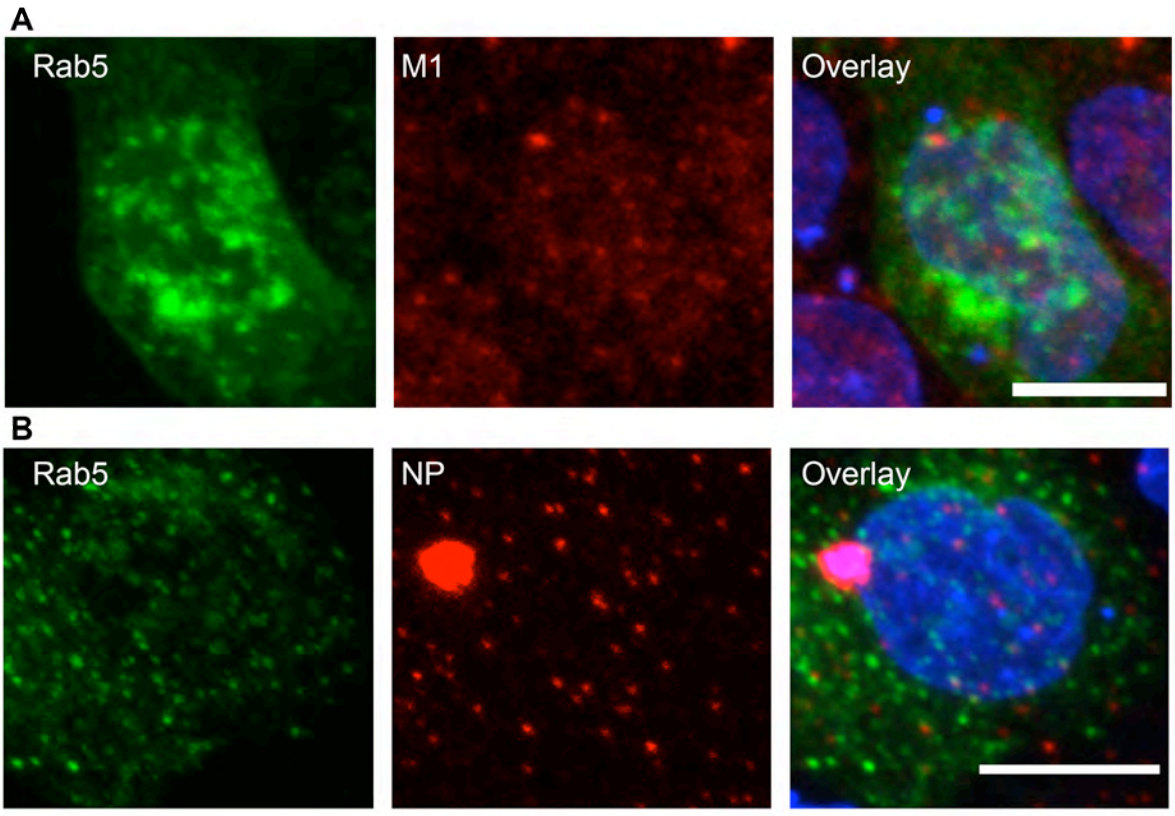

M1 and NP do not co-localize with endosomal marker Rab5-GFP after acid by-pass. MDCK cells were transfected with Rab5-GFP using TurboFect (*Thermo Scientific*) according to the manufacturer's protocol. After acid by-pass, the cells were fixed and immunostained using antibodies against the viral M1 (anti-goat A647) and NP (B) (anti-mouse A647). The cells were imaged using confocal microscopy. The figure shows a sum projection of slices through the whole cell. Both M1 and NP do not co-localize with the endosomal marker Rab5-GFP after acid by-pass.

Fig. S10

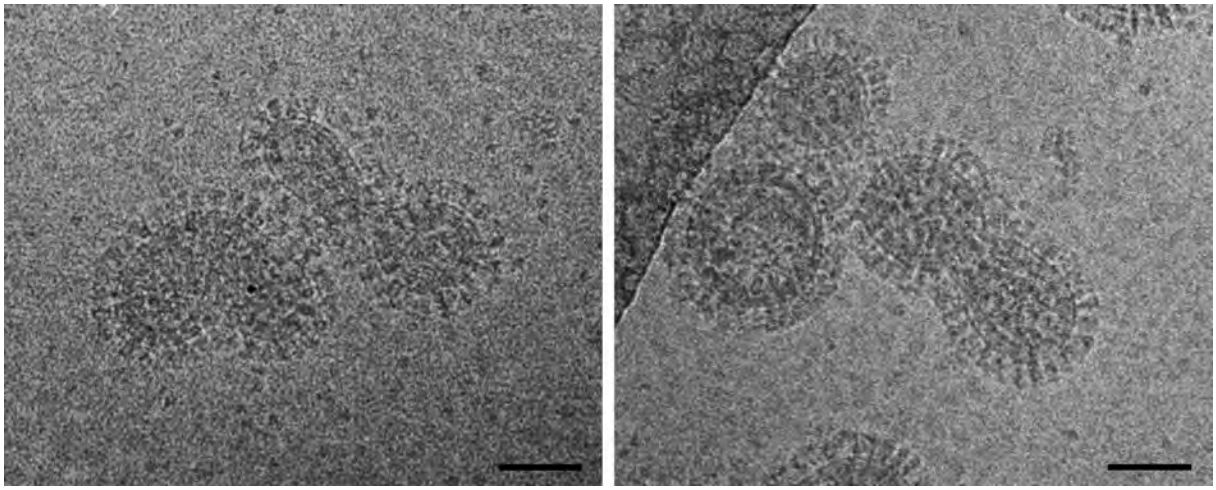

Effects of K^+/Ca^{2+} on virus morphology.
Cryo-electron micrographs of influenza A/X31 virus incubated 30 min at pH 7.4 (37°C) in PBS *with* **(left)** or *without* **(right)** high K^+ and high Ca^{2+} concentration. In both cases, the intact M1 layer is clearly visible suggesting no effect on the integrity of the M1 layer originating from the high potassium/calcium level.
Scale bars are 50 nm.

Fig. S11

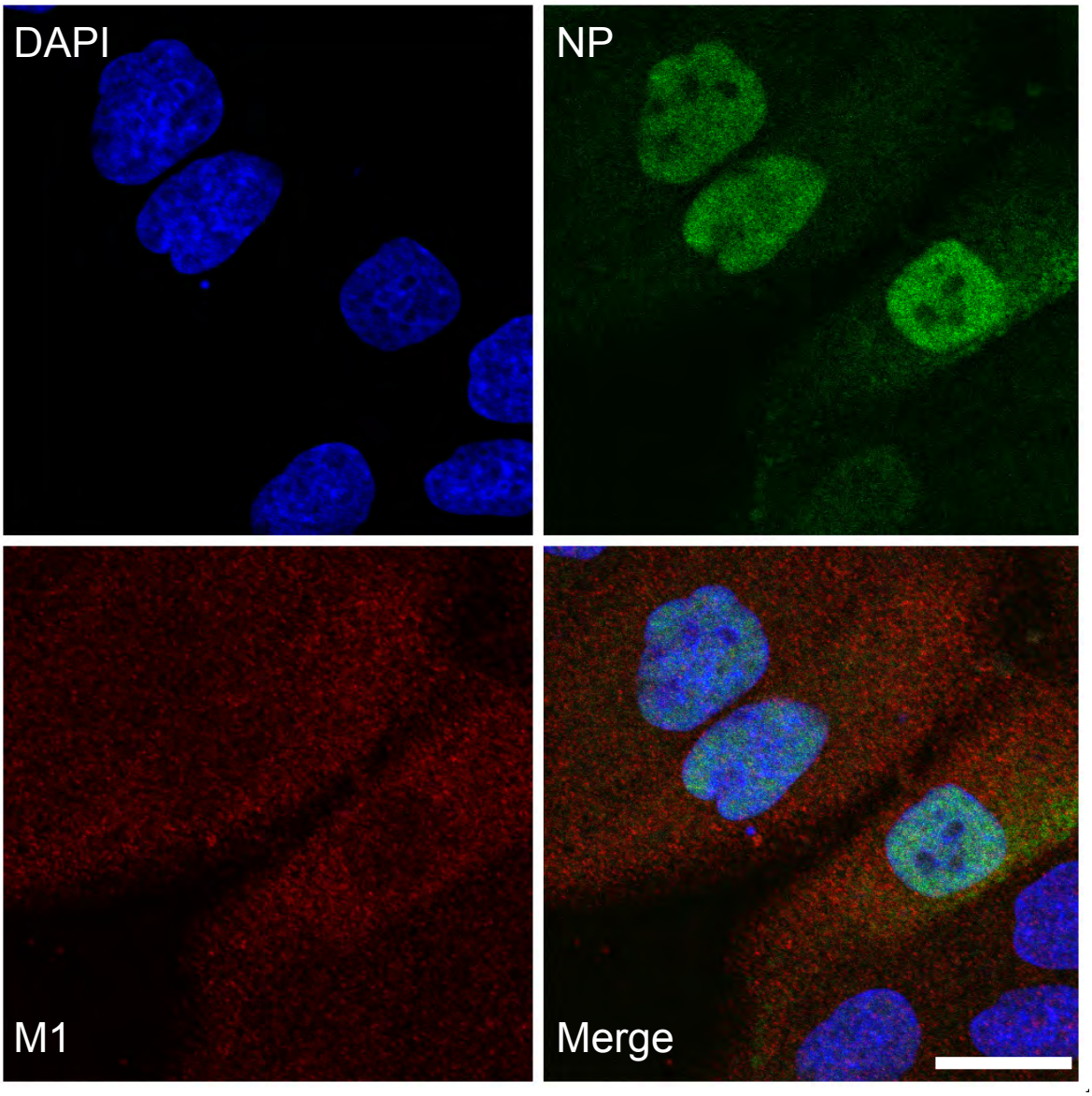

Localization of viral NP and M1 in MDCK cells 5 h post-infection with influenza A/Panama.
To investigate the localization of M1 and NP following a normal endocytic infection, MDCK cells were infected with influenza A/Panama/2007/99 for 5 h, fixed and stained against the viral NP and M1 protein. The nucleus was counterstained using DAPI. At this time, NP shows a strong accumulation in the nucleus with some NP already exported to the cytoplasm. M1 appears mostly cytosolic. Scale bar = 10 µm.

Fig. S12

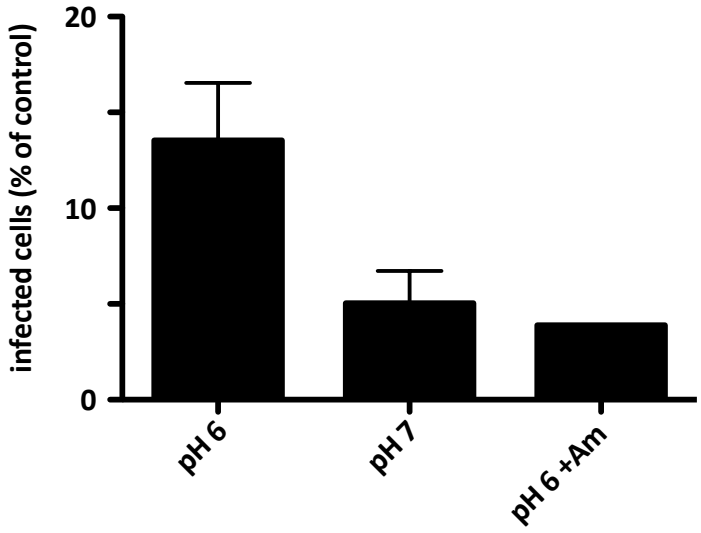

Infection efficiency of influenza A/Panama/2007/99 **in MDCK cells after pre-incubation at different conditions.**
The image-based analysis of influenza A virus infection efficiency confirms the supportive effect of a subacidic incubation step prior to HA-mediated fusion. Influenza viruses were pre-incubated at the indicated pH conditions, bound to MDCK cells on ice before acid-mediated by-pass was induced by adding a pH 5 buffer. The cells were incubated for 5 h in infection medium supplemented with 200 nM bafilomycin A. Cells and nuclei were identified using CellProfiler (7) and classified using CellProfiler Analyst as infected and not infected. Mean ± SEM (n=4).

Table S1

compared datasets	# s.e.m. difference (Δmean/∑s.e.m)	significance
A/X31 virus (pH 7.4) *vs.* A/Japan liposome (pH 7.4)	6.0	2e-9
bald A/X31 virus (pH 7.4) *vs.* A/Japan liposome (pH 7.4)	6.5	8e-11
A/X31 virus (pH 7.4) *vs.* bald A/X31 virus (pH 7.4)	0.68	0.50
bald A/X31 virus (pH 7.4) *vs.* bald A/X31 virus (pH 6.0)	1.64	0.10
bald A/X31 virus (pH 6.0) *vs.* bald A/X31 virus (pH 5.5)	1.85	0.06
bald A/X31 virus (pH 5.5) *vs.* bald A/X31 virus (pH 5.0)	0	1
bald A/X31 virus (pH 7.4) *vs.* bald A/X31 virus (pH 6.0 → 7)	0.27	0.79
infection efficiency after pH 6 vs. pH 7 pre-incubation	1.83	0.05

Table S5: Statistical analysis

To obtain a measure of the statistical relevance of the measured differences between the means of different datasets, we divided this difference by the sum of the respective s.e.m. values.

If standard errors did not overlap then the two datasets belong with a 0.32 probability to the same population. If also twice the s.e.m. did not overlap, the same probability was 0.05 etc. This calculation was made under the assumption of a normal distribution around the reciprocal fit.

The first column shows the two datasets that are compared. The second column shows the difference expressed by the sum of the two s.e.m. values. The third column gives the probability that both datasets belong to the same population, these values are calculated with the error function.

Supporting Materials and Methods

HA conformational change and fusion assay

HA conformational change within intact viruses was monitored at 37 °C using the environment-sensitive fluorophore bis-ANS (Invitrogen) as described previously (8). The bis-ANS quantum yield decreases upon water exposure, and it was shown to be sensitive to monitor HA conformational change also in intact viruses.

Fusion was measured by monitoring the fluorescence dequenching (FDQ) of the lipid-like fluorophore R18 (Invitrogen) upon fusion of R18-labeled viruses with ghost membranes at 37°C (9). The R18-labeled virus suspension (10 µl) was mixed with ghost suspension (40 µl) and incubated for 20 min at RT. Unbound virus was removed by centrifugation (5 min, 1200 g). The virus–ghost suspension was transferred to a glass cuvette containing prewarmed sodium acetate buffer, and the fluorescence was detected (λ_{ex} = 560 nm; λ_{em}= 590 nm) with a Horiba Jobin-Yvon FluoroMax spectrofluorometer. Fusion was triggered by the addition of citric acid. The suspension was continuously stirred with a 2 by 8 mm Teflon-coated magnetic stir bar. After 9 min the fusion was stopped by adding Triton X-100 (50 µl, final 0.5 %) to obtain the maximum R18 fluorescence.

Limited proteolysis of M1

For proteolysis of M1 at different pH and buffer conditions, N-terminally His-tagged M1 from Influenza A/FPV was recombinantly generated in *E.coli* Rosetta. M1 was expressed from plasmid pET15b (Novagen, Dramstadt, Germany), into which it was inserted using restriction sites *Nde*I and *Xho*I. After His-tag purification on TALON metal affinity columns (Clontech, Heidelberg, Germany), freshly prepared M1 (35 µM) was dialysed over night at 4 °C, using the Mini Dialysis Kit (1 kDa cut-off) from GE Healthcare (Freiburg, Germany) in order to adjust various buffer conditions for subsequent proteolysis. The following buffers were used: DPBS (1.5 mM KH_2PO_4, 8.1 mM Na_2HPO_4, 137 mM NaCl, 2.7 mM KCl) adjusted to pH 7.4 or pH 5 and potassium phosphate buffered saline with calcium (10 mM KPO_4, 150 mM KCl, 500 µM of $CaCl_2$) adjusted to pH 7.4, pH 6 or pH 5.

Proteinase K (0.5 µg/µl) was subsequently added to M1 at a molar enzyme-to-protein ratio of 1:100, and the samples were incubated for 20 min at RT. As control, part of each sample was incubated in the absence of enzyme. To concentrate the protein after enzymatic cleavage, 20 volumes of cold saturated ammonium sulphate solution were added, and samples were incubated for 30 min on ice. They were then centrifuged for 15 min at 16,000 x g, and the pellets were washed with ice cold acetone and centrifuged again. Finally, protein precipitates were resuspended in 80 µl of sample buffer and analyzed by reducing SDS-PAGE using 20 % polyacrylamid gels according to the protocol established by Schägger and Jagow (10). Protein bands were visualized by silver staining.

References

1. Muller, D. J., D. Fotiadis, S. Scheuring, S. A. Muller, and A. Engel. 1999. Electrostatically balanced subnanometer imaging of biological specimens by atomic force microscope. Biophysical journal 76:1101-1111.
2. Huang, Q., R. Opitz, E. W. Knapp, and A. Herrmann. 2002. Protonation and stability of the globular domain of influenza virus hemagglutinin. Biophysical journal 82:1050-1058.
3. Rachakonda, P. S., M. Veit, T. Korte, K. Ludwig, C. Bottcher, Q. Huang, M. F. Schmidt, and A. Herrmann. 2007. The relevance of salt bridges for the stability of the influenza virus hemagglutinin. Faseb J 21:995-1002.
4. Moncelli, M. R., L. Becucci, and R. Guidelli. 1994. The intrinsic pKa values for phosphatidylcholine, phosphatidylethanolamine, and phosphatidylserine in monolayers deposited on mercury electrodes. Biophysical journal 66:1969-1980.
5. Li, S., F. Eghiaian, C. Sieben, A. Herrmann, and I. A. Schaap. 2011. Bending and puncturing the influenza lipid envelope. Biophysical journal 100:637-645.
6. van Meer, G., D. R. Voelker, and G. W. Feigenson. 2008. Membrane lipids: where they are and how they behave. Nature reviews 9:112-124.
7. Carpenter, A. E., T. R. Jones, M. R. Lamprecht, C. Clarke, I. H. Kang, O. Friman, D. A. Guertin, J. H. Chang, R. A. Lindquist, J. Moffat, P. Golland, and D. M. Sabatini. 2006. CellProfiler: image analysis software for identifying and quantifying cell phenotypes. Genome biology 7:R100.
8. Korte, T., and A. Herrmann. 1994. pH-dependent binding of the fluorophore bis-ANS to influenza virus reflects the conformational change of hemagglutinin. Eur Biophys J 23:105-113.
9. Arbuzova, A., T. Korte, P. Muller, and A. Herrmann. 1994. On the validity of lipid dequenching assays for estimating virus fusion kinetics. Biochimica et biophysica acta 1190:360-366.
10. Schagger, H., and G. von Jagow. 1987. Tricine-sodium dodecyl sulfate-polyacrylamide gel electrophoresis for the separation of proteins in the range from 1 to 100 kDa. Analytical biochemistry 166:368-379.